 CMES, vol.77, no.3, pp.183-199, 2011

Experimental and Numerical Investigation of Instructions for Hyperelastic Membrane Inflation Using Fluid Structure Coupling

M.Souli[1] **and F.Erchiqui**[2]

Abstract: During the design process of membrane structure to resist to high pressure loading, and the characterization of hyperelastic material, a structure made up of thin rubber undergoes large deformation and rotation under high pressure loading out of high pressurized gas. Until recently, to simulate the inflation of the hyperelastic membrane, a uniform pressure based on thermodynamic model or experimental tests is applied to the structure, as boundary conditions. From a computational time point of view, this approach is very fast, since no computational fluid dynamics is involved in the simulation. However, at the late stage of the membrane inflation, uniform pressure simulations lead to numerical instability due to the lack of fluid that generates damping effects and prevent numerical instability. Thus the uniform pressure assumption is unstable at the end phase of the inflation for long time duration. To simulate accurately the inflation process, computational fluid dynamics in a moving fluid domain as well as fluid structure interaction (FSI) algorithms need to be performed for accurate pressure prediction and fluid structure interface coupling. For the simulation of gas dynamic in a moving domain, Arbitrary Lagrangian Eulerian (ALE) formulation is used. Both simulations, uniform pressure and ALE simulation for computational gas dynamics, were compared to test data, indicating satisfactory results in terms of correlation for earlier stage of the inflation. However for late stage inflation, simulation using uniform pressure show numerical instability leading to the blow up of the structure. With the more recently developed procedure, ALE theory, shows the greatest accuracy, both in terms of graphical and schematic comparison, especially at the late stage of the inflation process. As a result, the new simulation procedure model can be utilised to research into the effects of changing the designs of the membrane structure to resist to highly pressure loading on soft rubber material.

Keywords: ALE, Fluid Structure Interaction

[1] Universite de Lille1, LML UMR CNRS 8107 France
[2] Universite du Quebec en Abitibi-Temiscamingue Canada

1 Introduction

Simulation of Fluid Structure Interaction (FSI) problems becomes more and more the focus of computational engineering in the last years. The Lagrangian formulation, where the mesh moves with material is mainly used to solve problems in solid mechanics, and can be used for FSI problems. For small deformation, Lagrangian formulation can solve fluid structure interface and material boundary accurately, the main limitation of this formulation is mesh distortion for large deformation and moving structure, since the fluid is solved on a moving domain due to the structure motion. Various approaches have been investigated to solve FSI problems, one of the commonly used approach to solve these problems is the ALE formulation which has been used with success in the simulation of fluid with large motion such as sloshing fuel tank in automotive industry and bird impact in aeronautic industry. Various approaches have been investigated to solve FSI problems, including ALE muti-material formulation as in Aquelet et al. (2005) and Lagrangian formulations, Benson (1992). The ALE multi-material formulation used in this paper, and developed by the first author in LSDYNA code, has been validated for several academic and industrial applications. Once simulations are validated by experimental test results, it can be used as a design tool for the improvement of the structure involved.

In this paper the ALE formulation for the simulation of fluid dynamics problems, as well as the coupling algorithm are presented. The paper is concentrated on the validation of the methodology that has been implemented in an explicit finite element code for structural dynamic to be able to simulate fluid structure interaction problems, where the fluid mesh can be defined by an ALE or Eulerian mesh and the structure mesh as a Lagrangian deformable mesh. From an algorithmic point of view, a fluid element can contain more than one fluid material, for structure inflation in ambient air, an element may contain one or two different materials, inside structure pressurized gas and outside ambient air. During the simulation, state variables are computed and stored for each material in each element. An interface tracking algorithm based on Young's method is used to capture the interface between the two materials inside the element. This method was used successfully to model many industrial and academic applications as the sloshing tank problem. For the structure involved in the coupling a rubber material is used with Mooney–Rivlin constitutive material. For characterization of Mooney–Rivlin material constants under biaxial deformation, we consider the problem of bubble inflation described in Erchiqui et al. (2011). In this technique, applied blowing pressure and height at the hemispheric pole are recorded during testing. Bubble inflation is practical because it requires relatively simple devices. Moreover, it provides the best representation of actual deformation during the process. The analytical treatment of inflation is complicated due to non linearities in the material behavior and extensive deformation.

Numerical methods can be used to simulate and predict the membrane deformation process by solving nonlinear ordinary differential equations governing bubble motion, mathematical description of the ordinary differential equations are described in detail in Erchiqui et al. (2007).

In this paper, we describe in section 2, the ALE formulation of the Navier Stokes equation in a moving domain, and the advection algorithms used to solve mass, momentum and energy conservation. The detail of a new coupling method, Euler Lagrange Coupling algorithm, used at the fluid structure interface for structure loading is described at the end of section 2.. For the structure, the mechanical properties of Mooney-Rivlin material under biaxial deformation obtained by using bubble inflation technique, are described in section 3. The last section is devoted to validate the capability of the methodology by comparing predicted displacement time history with experimental data. Once simulations are validated by test results, it can be used as design tool for the improvement of the system structure involved.

2 ALE formulation and Coupling algorithm

2.1 ALE and Eulerian formulation

Fluid problems, in which interfaces between different materials (gas and ambient air) are present, are more easily modeled by using a Lagrangian mesh. However, if an analysis for complex tank geometry is required, the distortion of the Lagrangian mesh makes such a method difficult to use many re-meshing steps are necessary for the calculation to continue. Another method to use is the Eulerian formulation. This change from a Lagrangian to an Eulerian formulation, however, introduces two problems. The first problem is the interface trackin, Young (1982) and the second problem is the advection phase or advection of fluid material across element boundaries.

To solve these problems, an explicit finite element method for the Lagrangian phase and a finite volume method (flux method) for the advection phase are used. We can refer to several explicit codes such as Pronto, Dyna3D and LS-DYNA; see Hallquist (1998) for a full description of the explicit finite element method. The advection phase has been developed by the first author into the LS-DYNA code, extending the range of applications that can be used with the ALE formulation. Current applications include sloshing involving a ‘free surface’, and high velocity impact problems where the target is modeled as a fluid material, thus providing a more realistic representation of the impact event by capturing large deformations.

An ALE formulation contains both pure Lagrangian and pure Eulerian formulations. The pure Lagrangian description is the approach that: the mesh moves with the material, making it easy to track interfaces and to apply boundary conditions.

Using an Eulerian description, the mesh remains fixed while the material passes through it. Interfaces and boundary conditions are difficult to track using this approach; however, mesh distortion is not a problem because the mesh never changes. In solid mechanics a pure Eulerian formulation it is not useful because it can handle only a single material in an element, while an ALE formulation is assumed to be capable of handling more than one material in an element.

In the ALE description, an arbitrary referential coordinate is introduced in addition to the Lagrangian and Eulerian coordinates. The material derivative with respect to the reference coordinate can be described in (2.1). Thus substituting the relationship between the material time derivative and the reference configuration time derivative derives the ALE equations.

$$\frac{\partial f(X_i,t)}{\partial t} = \frac{\partial f(x_i,t)}{\partial t} + w_i \frac{\partial f(x_i,t)}{\partial x_i} \tag{2.1}$$

where X_i is the Lagrangian coordinate, x_i the Eulerian coordinate, w_i is the relative velocity. Let denote by v the velocity of the material and by u the velocity of the mesh. In order to simplify the equations we introduce the relative velocity $w = v - u$. Thus the governing equations for the ALE formulation are given by the following conservation equations (2.2) to (2.4):

(i) *Mass equation.*

$$\frac{\partial \rho}{\partial t} = -\rho \frac{\partial v_i}{\partial x_i} - w_i \frac{\partial \rho}{\partial x_i} \tag{2.2}$$

(ii) *Momentum equation.*

The strong form of the problem governing Newtonian fluid flow in a fixed domain consists of the governing equations and suitable initial and boundary conditions. The equations governing the fluid problem are the ALE description of the Navier-Stokes equations:

$$\rho \frac{\partial v_i}{\partial t} = \sigma_{ij,j} + \rho b_i - \rho w_i \frac{\partial v_i}{\partial x_j} \tag{2.3}$$

The stress tensor σ_{ij} is described as follows:

Boundary and initial conditions need to be imposed for the problem to be well posed.

The superscript means prescribed value, n_i is the outward unit normal vector on the boundary, and δ_{ij} is Kronecker's delta function.

(iii) *Energy equation.*

$$\rho \frac{\partial E}{\partial t} = \sigma_{ij} v_{i,j} + \rho b_i v_i - \rho w_j \frac{\partial E}{\partial x_j} \tag{2.4}$$

Note that the Eulerian equations commonly used in fluid mechanics by the CFD community, are derived by assuming that the velocity of the reference configuration is zero and that the relative velocity between the material and the reference configuration is therefore the material velocity. The term in the relative velocity in (2.3) and (2.4) is usually referred to as the advective term, and accounts for the transport of the material past the mesh. It is the additional term in the equations that makes solving the ALE equations much more difficult numerically than the Lagrangian equations, where the relative velocity is zero.

In the second phase, the advection phase, transport of mass, internal energy and momentum across cell boundaries are computed; this may be thought of as remapping the displaced mesh at the Lagrangian phase back to its original or arbitrary position.

From a discretization point of view of (2.2) , (2.3) and (2.4), one point integration is used for efficiency and to eliminate locking,. The zero energy modes are controlled with an hourglass viscosity Benson (1992). A shock viscosity, with linear and quadratic terms, is used to resolve the shock wave, Richtmyer et al. (1967); a pressure term is added to the pressure in the energy equation (2.4). The resolution is advanced in time with the central difference method, which provides a second order accuracy in time using an explicit method in time. For each node, the velocity and displacement are updated as follows:

$$u^{n+1/2} = u^{n-1/2} + \Delta t.M^{-1}.(F_{exl} + F_{int}) \tag{2.5a}$$

$$x^{n+1} = x^{n-1} + \Delta t.u^{n+1/2} \tag{2.5b}$$

The multi-material formulation is attractive for solving a broad range of non-linear problems in fluid and solid mechanics, because it allows arbitrary large deformations and enables free surfaces to evolve. The Lagrangian phase of the VOF method is easily implemented in an explicit ALE finite element method. Before advection, special treatment for the partially voided element is needed. For an element that is partially filled, the volume fraction satisfies $V_f \leq 1$, and the total stress by σ is weighed by volume fraction $\sigma_f = \sigma.V_f$.

In the second phase, the transport of mass, momentum and internal energy across the element boundaries is computed. This phase may be considered as a 're-mapping' phase. The displaced mesh from the Lagrangian phase is remapped into the initial mesh for an Eulerian formulation, or an arbitrary undistorted mesh for an ALE formulation.

In this advection phase, we solve a hyperbolic problem, or a transport problem, where the variables are density, momentum and internal energy per unit volume. Details of the numerical method used to solve the equations are described in detail

in Aquelet et al. (2005), where the Donor Cell algorithm, a first order advection method and the Van Leer algorithm, a second order advection method are used. As an example, the equation for mass conservation is:

$$\frac{\partial \rho}{\partial t} + \nabla.(\rho u) = 0 \tag{2.6}$$

It is not the goal of this paper to describe the different algorithms used to solve equation (3.1); these algorithms have been described in detail in Benson (1992) and Aquelet et al. (2005). Figure 1 describes the two phases for a one step explicit calculation.

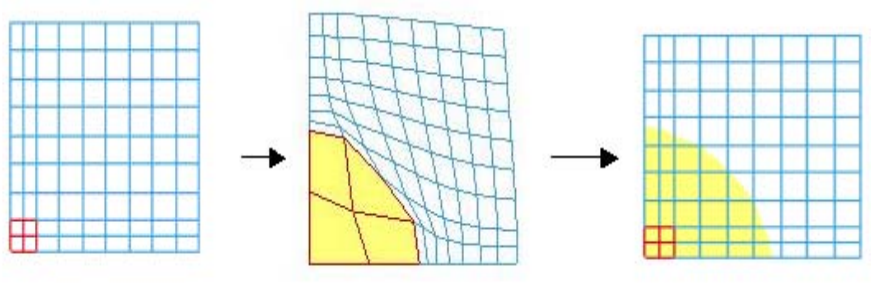

Lagrangian Phase Advection phase

Figure 1: Lagrangian and Advection phases in multi-material ALE formulation

2.2 Coupling Algorithm

Several coupling methods between CFD and structural dynamic solvers have been developed to solve coupling problems. Classical implicit and explicit coupling are described in detail in Longatte et al. (2003) and Longatte et al. (2009), where hydrodynamic forces from the fluid solver are passed to the structure solver for stress and displacement computation. In this paper, a coupling method based on contact algorithm is used. Since the coupling method described in this chapter is based on the penalty method for contact algorithms, the contact approach is a good introduction to this method. In contact algorithms, a contact force is computed proportional to the penetration vector, the amount the constraint is violated. In an explicit FEM method, contact algorithms compute interface forces due to impact of the structure on the fluid, these forces are applied to the fluid and structure nodes in contact in order to prevent a node from passing through contact interface. In contact algorithms, one surface is designated as a slave surface, and the second as

a master surface. The nodes lying on both surfaces are also called slave and master nodes respectively. The penalty method imposes a resisting force to the slave node, proportional to its penetration through the master segment , as shown in figure 2a describing the contact process. This force is applied to both the slave node and the nodes of the master segment in opposite directions to satisfy equilibrium.

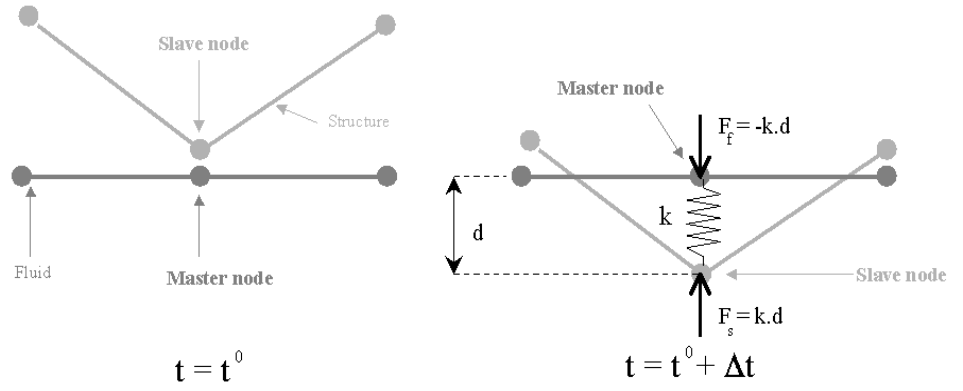

(a)

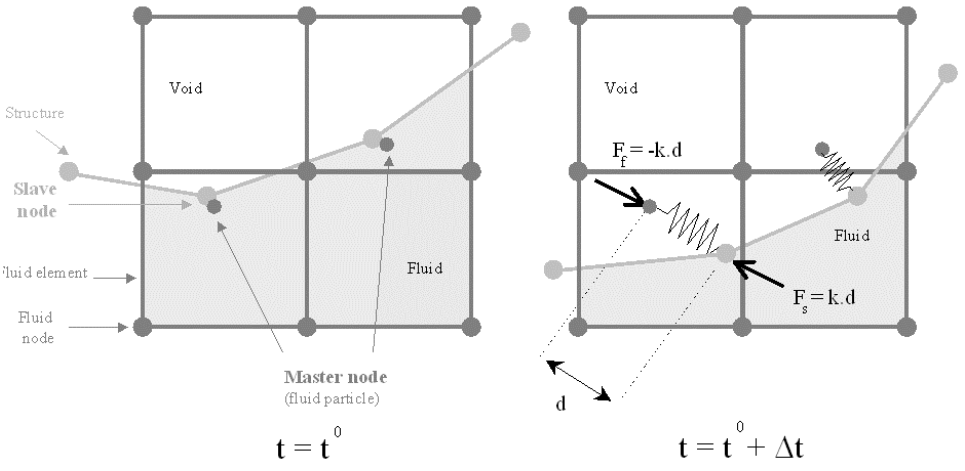

(b)

Figure 2: a. Description of Penalty Contact algorithm; b. Description of Penalty Coupling algorithm

Penalty coupling behaves like a spring system and penalty forces are calculated proportionally to the penetration depth and spring stiffness. The head of the spring

is attached to the structure or slave node and the tail of the spring is attached to the master node within a fluid element that is intercepted by the structure, as illustrated in figure 2b.

Similarly to penalty contact algorithm, the coupling force is described by (2.7):

$$F = k.d \tag{2.7}$$

where k represents the spring stiffness, and d the penetration. The force F in figure 2b is applied to both master and slave nodes in opposite directions to satisfy force equilibrium at the interface coupling, and thus the coupling is consistent with the fluid-structure interface conditions namely the action-reaction principle.

The main difficulty in the coupling problem comes from the evaluation of the stiffness coefficient k in Eq. (2.7). The stiffness value is problem dependent, a good value for the stiffness should reduce energy interface in order to satisfy total energy conservation, and prevent fluid leakage through the structure. The value of the stiffness k is still a research topic for explicit contact-impact algorithms in structural mechanics. In this paper, the stiffness value is similar to the one used in Lagrangian explicit contact algorithms, described in Benson (1992). The value of k is given in term of the bulk modulus K of the fluid element in the coupling containing the slave structure node, the volume V of the fluid element that contains the master fluid node, and the average area $A$of the structure element connected to the structure node.

$$k = p_f.\frac{K.A^2}{V} \tag{2.8}$$

3 Characterization of constitutive material and experimental setup

3.1 Characterization of constitutive material

First, we need to characterize material data using a bubble inflation technique, Joye et al. (1972) to fit the constitutive model. To get material properties constants of the membrane structure, The experimental setup has been described in detail in Erchiqui et al. (2001), using the experimental setup in figure 3. Hyperelastic constants were determined by biaxial characterization: membrane is subjected to free inflation (with a controlled air flow rate) while the forming pressure and bubble height were measured.

A hyperelastic material is defined as an elastic material in which the stress at each point can be derived from a scalar function W(**F**) called the strain energy function. In order to meet the requirements of objectivity, the strain energy function must be invariant under changes in the observer frame of reference. It is well known that the

Cauchy–Green deformation tensor is invariant under changes in the observer frame of reference. Thus, if the strain energy function can be written as a function of the right Cauchy–Green tensor **C**, it automatically meets the objectivity principle. The general stress–strain relationship is given by the formula (3.1):

$$S_{ij} = 2\frac{\partial W}{\partial C_{ij}} \tag{3.1}$$

where **S** is the Piola–Kirchhoff stress tensor. The different models in the literature define the strain energy as a function of the strain field. We considere the Rivlin's theory, Rivlin (1948). Rivlin's theory of isotropic materials describes the energy as a function of the three Cauchy strain invariants I_1, I_2, and I_3. Assuming material incompressibility, the stress can be obtained from the following Mooney–Rivlin form (3.2):

$$W = \sum_{i+j=1}^{N} C_{ij}\,(I_1 - 3)^i\,(I_2 - 3)^j \tag{3.2}$$

The use of two terms in the series is sufficient to describe the elastic modulus in both the uniaxial and biaxial deformation modes. The tangential stresses T_1 and T_2 are deduced from the following expression for the strain energy W.

3.2 Experimental and numerical identification

Erchiqui et al. (2001), and Virk et al. (2009), have investigated experimentally and numerically inflation behavior in thermoplastic membrane under the combined effects of applied stress and temperature using bubble inflation tests. The results were used to identify the material constants embedded in the constitutive models of polymeric materials in this work. The polymeric material, acrylonitrile-butadiene-styrene (ABS), was tested under biaxial deformation using bubble inflation technique. Initial ABS sheet thickness was 1.57 mm. The experimental setup is described in figure 3, where a circular membranes were mounted between two metal disks containing a circular aperture and clamped onto a support. The exposed circular area of diameter D=15cm cm was heated to softening point in an infrared heating chamber. When the temperature became uniform over the flat sheet, the circular area was inflated using compressed air at a controlled flow rate. During testing, the applied blowing pressure, which was uniform over the membrane, was measured with a pressure sensor. Height at the hemispheric pole, the center of the membrane, and time were recorded simultaneously using a video camera and a data acquisition system.

For most inflation tests, testing ends when the bubble bursts. Figure 4 shows the inflation profile of a circular plane membrane. Figure 5 shows the experimental and fitting bubble height vs. time data at the pole of the membrane for ABS at 145^{o}C.

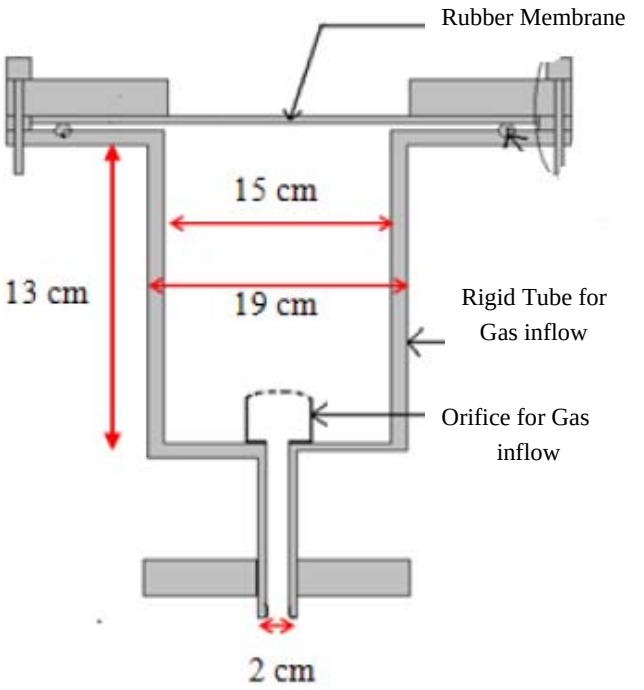

Figure 3: Description of the experimental Setup

Figure 6 compares the predicted pressure versus bubble height data at the pole of the bubble using the Mooney–Rivlin model for the experimental measurements of ABS at 145^{o}C. The measurement error is smaller during the pressure rise ($\approx$5%). However, the numerical model for ABS provides a better fit to the experimental data, as can be seen in Figure 5. It should be noted that at maximum pressure the bubble height is of the order of the initial membrane radius. Beyond this critical point, the height increases rapidly while the pressure falls. This unstable behavior continues until the bubble bursts.

4 Numerical simulations

As a validation of the formulation described above, we first consider the problem of free blowing of a viscoelastic membrane. The geometry of the structure is modeled

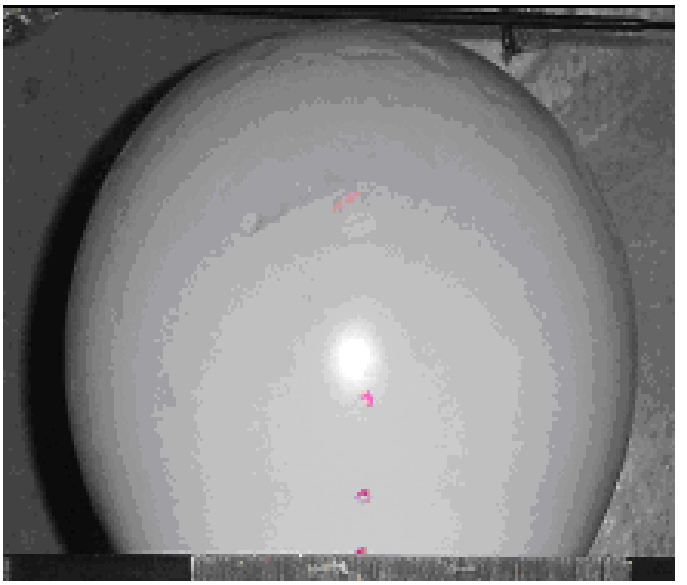

Figure 4: Inflation of a flat circular membrane, ABS

using quarter symmetry model, and meshed with 4 nodes shell elements (2733 nodes and 132 shell elements) is considered as shown in Figure 11.

The measured pressure was interpolated by a polynomial function (Figure 7) and used in the finite element program (Lagrangian Formulation) to compute the time evolution of the bubble height at the pole. The predictions obtained with Mooney-Rivlin model give almost identical results and is shown against experimental data in Figure 7, at a setting temperature of 143^oC. We notice that the Mooney-Rivlin model predict similar bubble height at the pole, which is close to the experimental measurements. However, the model gives different results, although close to the experimental measurements, when the bubble pressure level is close to the maximum pressure reached during experiments. This phenomenon is related to the models used and is the subject of several studies. Indeed, for these models there exists a critical pressure beyond which the system diverges (unstable branch). The work as presented does not, for now, describe the unstable region of the solution.

To validate the numerical results and to prove the ability of the ALE fluid structure coupling method to solve problems where the classical pressure boundary conditions cannot, we use the two types of material with different Moony Rivlin Coefficients, C01=115590 Pas and C01=105010 Pas. For the first material with C01=115590 Pas, both formulations give same results and good correlation with experimental data. The correlation can be seen in figure 8, where the evolution

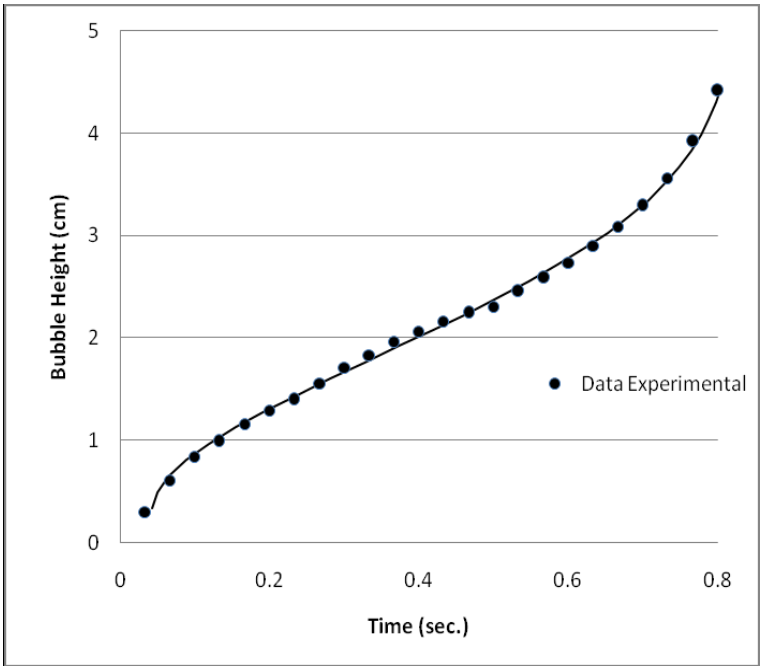

Figure 5: Experimental and predicted pressure versus bubble height for ABS at 147 ^{o}C

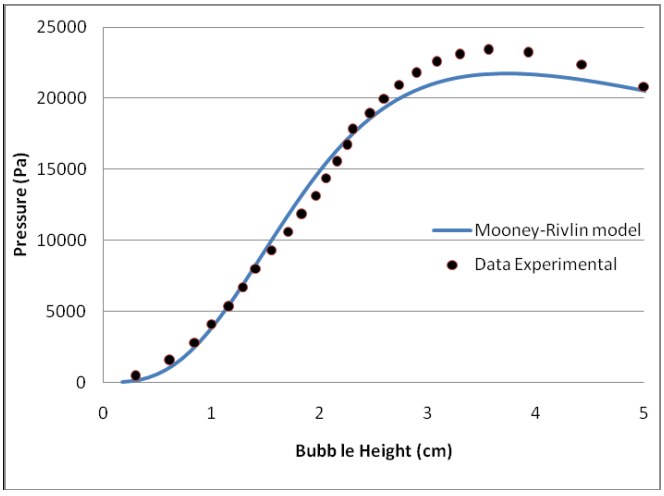

Figure 6: Experimental and predicted pressure versus bubble height for ABS at 147 ^{o}C

of the bubble height at the center of the membrane structure versus time is plotted for experimental test and numerical simulation. For the softer material with C01=105010 Pas, the solution from the simulation using pressure boundary condition and no fluid, becomes unstable after t=0.6 second. This instability has not been shown in our experimental tests when using this material. This instability is due to the lack of damping that can be provided by the fluid. The missing fluid in the pressure boundary condition simulation creates a lack of damping in the system that lead the structure to numerical instability. This instability did not show up in the simulation using fluid structure coupling, since the fluid involved in the simulation has a damping effect during inflation. For this material, with C01=105010 Pas, time evolution of the bubble height for both simulations is plotted in figure 9. In this figure, we can see the instability after t=0.6 second of the simulation using pressure boundary condition.

Figures 10 to 12 present the evolution of the extension at 0 sec, 0.129 sec and 0.6 sec, respectively, associated with Mooney-Rivlin model using C01=105010. In Figure 11, we present the final Von Mises stress distribution at t=0.6 second. Let us notice that ALE formulation has been used successfully for different fluid structure coupling applications including metal forming , Gakwaya et al. (2011), and turbulent flow, Naji et al. (2009)

These simulations are of great interest for the design of monument to resist a blast and provide protection to the monument and its occupants. Since the ultimate objective is the design of monument with occupant safety, numerical simulations can be included in shape design optimization with shape optimal design techniques, souli et al. (1993), and material optimization, Erchiqui et al. (2007). Once simulations are validated by test results, it can be used as design tool for the improvement of the system structure involved.

5 Conclusion

In this work, we have presented the application of a Arbitray Lagrangian Eulerian (ALE) approach ALE for simulating the response of isotropic, incompressible thermoplastic material. The experimental validation is performed for an ABS material, in the case of free inflation of a circular membrane subject to a dynamical pressure load distribution.

The simulations were compared to test data, indicating satisfactory results in terms of correlation, with the more recently developed procedure, ALE theory, showing the greatest accuracy, both in terms of graphical and schematic comparison, especially in the late stage of the inflation process. We have shown that the fluid structure coupling method, using ALE formulation where the fluid is represented

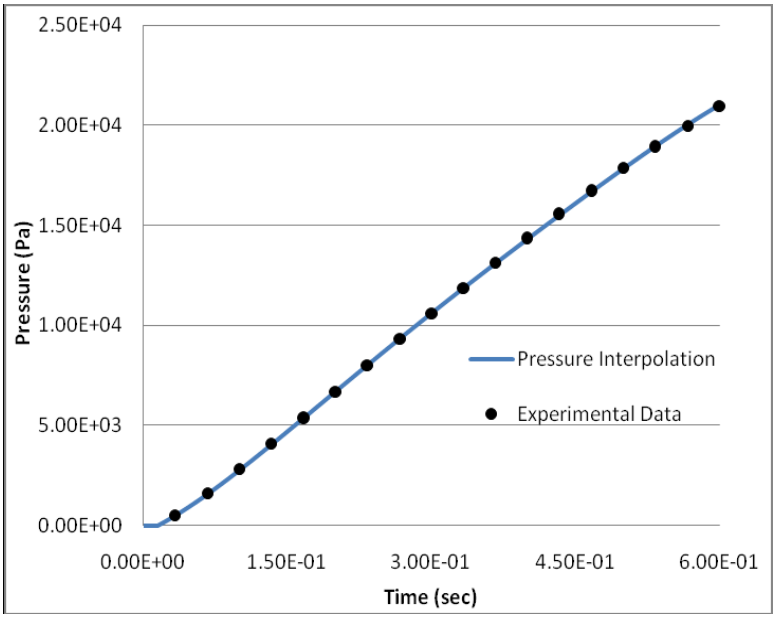

Figure 7: Pressure interpolation versus experimental data and time

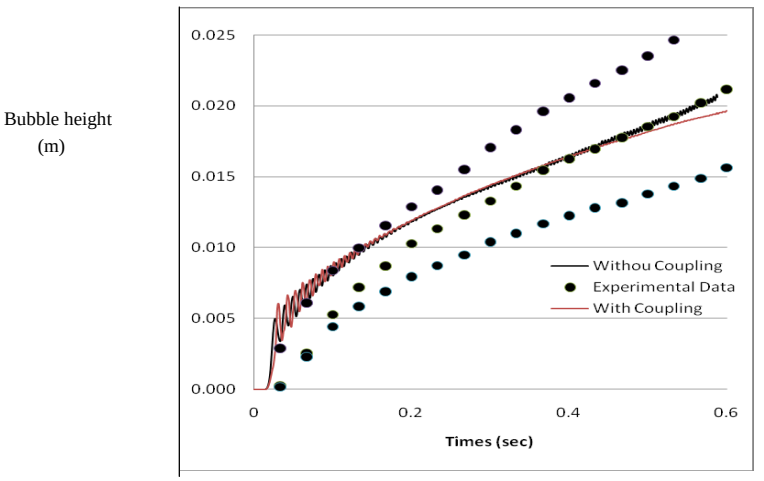

Figure 8: Bubble height time evolution C01=115590 Pa

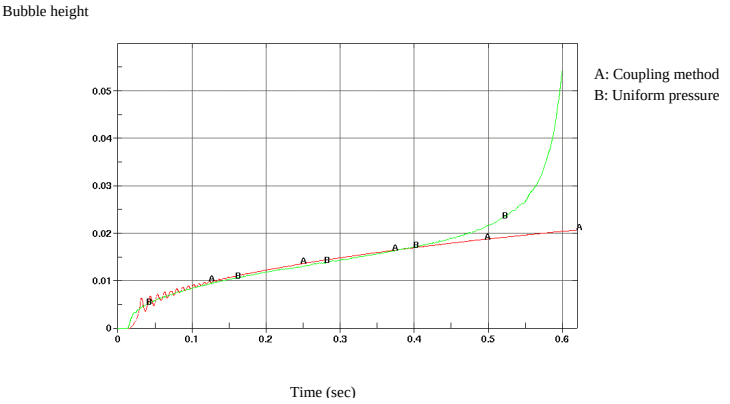

Figure 9: Bubble height time evolution C01=105010

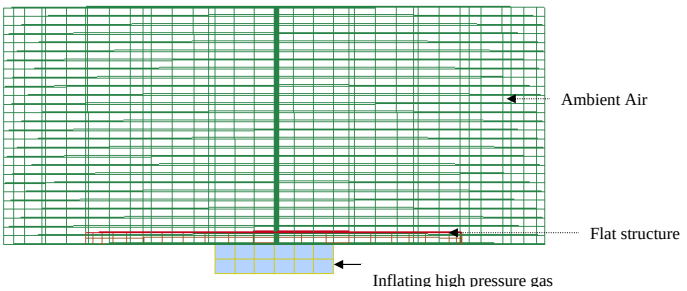

Figure 10: Initial ALE Fluid Mesh overlapping structure mesh

by the full hydrodynamic equations can be more accurate and also more stable that the Lagrangian method using pressure boundary conditions. Numerical simulation using coupling method can still be stable for low Young modulus of the structure, whereas the simulation using Lagrangian formulation with pressure boundary conditions is unstable and cannot represent physical phenomena for soft rubber structure. As a result, the new simulation procedure model can be utilised to research into the effects of changing the designs of the membrane structure to resist to highly pressure loading.

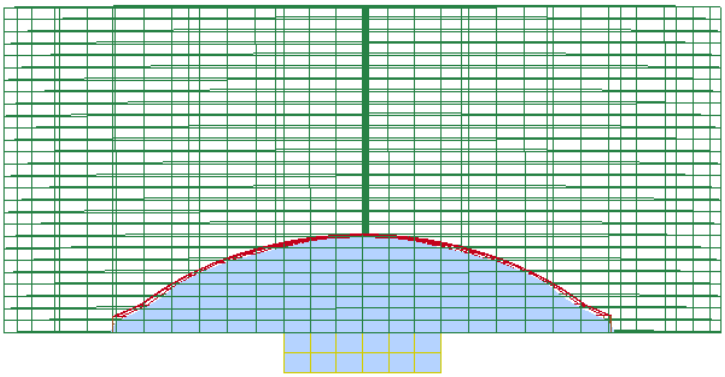

Figure 11: Fluid Material and structure displacement at t=0.129s

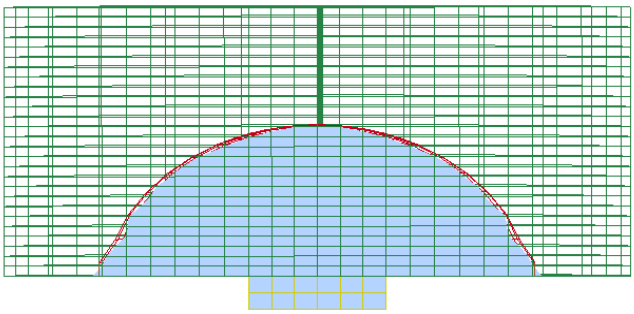

Figure 12: Fluid Material and structure displacement at t=0.6s

References

Aquelet, N; Souli, M; Olovson, O, (2005): Euler Lagrange coupling with damping effects: Application to slamming problems. *Computer Methods in Applied Mechanics and Engineering*, Vol. 195, pp 110-132.

Benson, D.J. (1992): Computational Methods in Lagrangian and Eulerian Hydrocodes. *Computer Methods in Applied Mech. and Eng.*, 99, 235-394.

Erchiqui, F.; Derdouri, A.; Gakwaya. A., and Verron E. (2001): Analyse expérimentale et numérique en soufflage libre d'une membrane thermoplastique. *En-*

tropie, Vol. 37, No. 235/236, pp. 118-125.

Erchiqui F. ; Souli M. ; Ben Yedder R. (2007) Nonisothermal finite-element analysis of thermoforming of polyethylene terephthalate sheet: Incomplete effect of the forming stage. *Polymer Engineering and Science*, Volume 47 Issue 12 pp. 2129-2144.

Gakwaya, A.; Sharifi, H.; Guillot; M. Souli, M.; Erchiqui, F (2011): ALE Formulation and Simulation Techniques in Integrated Computer Aided Design Engineering System with Industrial Metal Forming Applications. *CMES: Computer Modeling in Engineering & Sciences*, Volume: 73 Issue: 3 pp 209-266.

Hallquist, J.O. (1998): *LS-DYNA theoretical manual Livermore Software Technology Company California USA*

Joye, D.D.; Poehlein, G.W; and Denson C.D., (1972): A bubble inflation technique for the measurement of viscoelastic properties in equal biaxial extension flow II. *Trans. Soc. Rheol.*, 16, pp. 421-445.

Longatte, E; Bendjeddou, Z; Souli, M. (2003): Application of Arbitrary Lagrange Euler Formulations to Flow-Induced Vibration problems. *Journal of Pressure Vessel and Technology*, Volume 125 Issue: 4, pp 411-417.

Longatte, E; Verreman, V; Souli, M. (2009): Time marching for simulation of Fluid-Structure Interaction Problems. *Journal of Fluids and Structures*, Volume 25, Issue 1, pp. 95-111.

Naj H.; Mompean , M. (2009): Computation of the Turbulent Flow in a Square Duct Using a Cubic Low-Reynolds Stress Model. *CMES: Computer Modeling Engineering & Sciences*, Volume: 53 Issue: 2 pp 181-206.

Richtmyer, R.D. and Morton, K.W., (1967): *Difference Equations for Initial-Value Problem. Interscience Publishers, New York.*

Rivlin, R.S., (1948): Large Elastic Deformation of Isotropic Materials – IV: Further Developments of the General Theory. *Phil. Trans. R. Soc.*, A241: 379–397.

Souli M.; Zolesio J.P. (1993): Shape Derivative of Discretized Problems. *Computer Methods in Applied Mechanics and Engineering*, Volume 108, Issue: 3-4, pp. 187–199

Virk N.M.S; Y. Mustaf Y.; E. Holdø A.E. (2009): Numerical analyses of a PEM fuel cell's performance having a perforated type gas flow distributor. *The International Journal of Multiphysics*, Volume 13 Num 4 pp: 347-360.

Young, D.L. (1982): Time-dependent multi-material flow with large fluid distortion, *Numerical Methods for Fluids Dynamics.* Ed. K. W. Morton and M.J. Baines, Academic Press, New-York.